Anisotropic Magnetoelastic Phenomena in Layered Manganite Crystals: Implication of Change in Orbital State

T. Kimura,[1] Y. Tomioka,[1] A. Asamitsu,[1,*] and Y. Tokura[2]
[1]*Joint Research Center for Atom Technology (JRCAT), Tsukuba 305-0046, Japan*
[2]*Department of Applied Physics, University of Tokyo, Tokyo 113-0033, Japan*
(Received 8 September 1998)

Magnetoelastic phenomena correlated with magnetoresistive ones have been investigated for bilayered manganite crystals, $La_{2-2x}Sr_{1+2x}Mn_2O_7$ ($0.3 \leq x \leq 0.45$), by measurements of the striction parallel and perpendicular to the MnO_2 plane in magnetic fields. The magnetization process causes not only a large negative magnetoresistance but also a gigantic lattice striction which is highly anisotropic with respect to the crystal axes. The magnitude and the sign of the lattice striction systematically varies with the doping level (x), which should reflect variation of the orbital-dependent occupancy in the two-dimensional conduction band with temperature, magnetic field, and doping level. [S0031-9007(98)08032-6]

PACS numbers: 75.80.+q, 72.15.Gd, 75.30.–m

Doped perovskite manganites show a wide variety of magnetic-field induced phenomena, including colossal magnetoresistance (CMR). Recent extensive studies have revealed that the observed features can be attributed not only to the double-exchange (DE) interaction [1] but also to other instabilities competitive with the DE interaction, such as the antiferromagnetic (AFM) superexchange, Jahn-Teller (JT), charge-orbital ordering interactions, etc. Some of these competing interactions strongly couple with the lattice through the orbital degrees of freedom (or JT effect) of the e_g electrons on Mn^{3+} ions. As illustrated in Fig. 1(a), since nearly degenerate e_g orbitals have lobes directed to the ligands (oxygen sites), the $3d$-$2p$ electron hybridization, as well as its anisotropy, is strongly dependent on the respective Mn-O bond lengths. The orbital degeneracy, and its lifting in a deformable lattice, lead to a variety of electronic/lattice instabilities and modifications. Thus, the study of magnetoelastic effects produced by the strong spin-charge-lattice coupling is expected to clarify the role of orbital degrees of freedom in charge-transport and magnetic properties in the manganite system.

Recently, intensive studies [2–6] have also been performed for the $n = 2$ member of the Ruddlesden-Popper series of manganites, $La_{2-2x}Sr_{1+2x}Mn_2O_7$, which exhibit the CMR effect as well. One of the most distinct features for the bilayered manganite is its anisotropic characteristics in charge-transport and magnetic properties. In the light of the aforementioned orbital degrees of freedom, the layered structure should bias the crystal field and hence lift, more or less, the degeneracy of the e_g orbital states, namely the $3d_{x^2-y^2}$ and $3d_{3z^2-r^2}$ conduction bands [see Fig. 1(a)]. However, the respective-orbital related bands should show different band dispersions along the inplane k vector [7,8], as schematically depicted in Fig. 1(a). The occupancy in the respective bands, which is primarily governed by the doping level x (or the band filling) and the crystal field (e.g., MnO_6 deformation), affects the total electronic energy and the magnetic interaction. In this Letter, we report on a gigantic and anisotropic magnetoelastic effect of $La_{2-2x}Sr_{1+2x}Mn_2O_7$ crystals over a wide composition range, that is a manifestation of the complex but unconventional interplay among spin, charge, and orbital degrees of freedom.

Single crystals of $La_{2-2x}Sr_{1+2x}Mn_2O_7$ ($0.3 \leq x \leq 0.45$) were grown by the floating zone method, as described in detail elsewhere [9]. The grown crystals were characterized by four-circle single-crystal x-ray diffraction (XRD) measurements which gave the bilayer structure

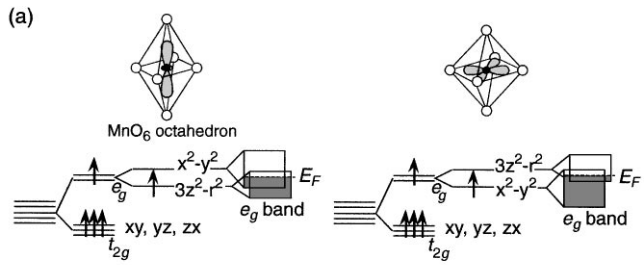

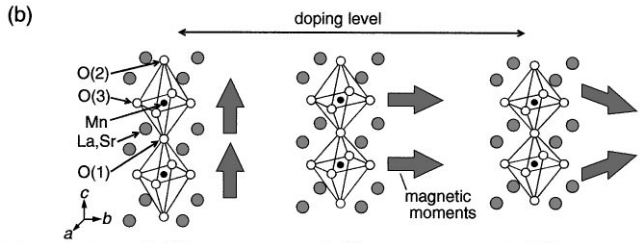

hole content	x~0.3	x~0.4	x~0.45
a_0 [Å]	3.860(2)	3.876(2)	3.878(1)
c_0 [Å]	20.380(2)	20.140(2)	20.053(2)
Mn-O(1) [Å]	1.98	1.95	1.94
Mn-O(2) [Å]	2.06	2.00	1.97
Mn-O(3) [Å]	1.93	1.94	1.94

FIG. 1. (a) Schematic electronic structure of Mn^{3+} ion in MnO_6 octahedron with JT distortion. The inplane e_g band in the layered manganite shows a different band dispersion and bandwidth depending on the respective orbital states. (b) Doping-level dependence of lattice distortion at room temperature in $La_{2-2x}Sr_{1+2x}Mn_2O_7$. Thick arrows on the right hand of respective crystal structures indicate the spin structures within a bilayer unit at low temperatures.

 0031-9007/98/81(26)/5920(4)$15.00

with the $I4/mmm$ tetragonal unit cells ($Z = 2$). The crystals were oriented using Laue XRD patterns, and cut into parallelepipeds along the main crystalline axes. Sample dimensions for the resistivity (ρ) and striction ($\Delta L/L$) measurements were typically $\sim 2 \times \sim 2 \times \sim 0.3$ mm^3, with the longest axes both parallel and perpendicular to the MnO_2 (ab) plane for the inplane ($\| ab$) and interplane ($\| c$) measurements, respectively. Resistivity measurements were made by a standard dc four-probe technique. The electrodes on the sample were formed by heat treatment type silver paint. The striction was measured using a uniaxial strain gauge with the length of 0.2 or 0.5 mm which was attached to the widest face of the specimen.

We show in Fig. 1(b) the schematic lattice distortion, lattice parameters, and Mn-O bond lengths of $x = 0.3$, 0.4, and 0.45 crystals at room temperature, obtained by four-circle single-crystal XRD measurements. The lattice parameter of the $a(b)$ axis slightly increases with increase of x, whereas that of the c axis decreases more rapidly. Variation of the lattice parameters is closely connected with that of the Mn-O bond lengths. The Mn-O(3) bond length along the $a(b)$ axis inconsiderably elongates with increasing x, while the Mn-O(2) bond length along the c axis steeply shrinks. The results are consistent with those from powder neutron studies [10]. Since the decrease of x corresponds to the e_g-electron doping, the systematic change of the Mn-O bond lengths reflects the orbital-state occupancy of the e_g electrons. A remarkable expansion of the out-of-plane Mn-O(2) bond length with lower hole concentration x (or higher electron concentration) implies that the doped electrons prefer to occupy the $3z^2 - r^2$ orbital-state [left panel in Fig. 1(a)].

Thick arrows on the right hand of the respective schematic crystal structures in Fig. 1(b) illustrate a variation of the low-temperature spin structure within a bilayer unit as a function of the doping level, which has been revealed by recent neutron diffraction studies [11–13]. The magnetic moments at the ground state always couple ferromagnetically within the constituent *single* MnO_2 layer. However, the coupling between the respective MnO_2 layers within a bilayer unit depends on the doping level. In a low-doped region around $x \approx 0.3$, the magnetic moments of respective *single* MnO_2 layers couple ferromagnetically within a bilayer, and align along the c axis. With increasing x, however, the magnetic moments direct along the ab plane and show canted antiferromagnetism beyond $x \approx 0.4$.

Temperature profiles of the striction along the ab plane [$\Delta L_{ab}(T)/L_{ab}(200\ \mathrm{K})$] and the c axis [$\Delta L_c(T)/L_c(200\ \mathrm{K})$] for these crystals are given in Figs. 2(a) and 2(b), respectively. The arrows indicate the magnetic transition temperature T_c. The T_c reaches the highest value ($\approx$130 K) around $x \approx 0.36$ as a function of x. The suppression of T_c toward higher x above $x \approx 0.36$ may be correlated with the aforementioned evolution of AFM coupling between the constituent single MnO_2 layers. The crystals with $0.3 \leq x \leq 0.4$ show distinct anoma-

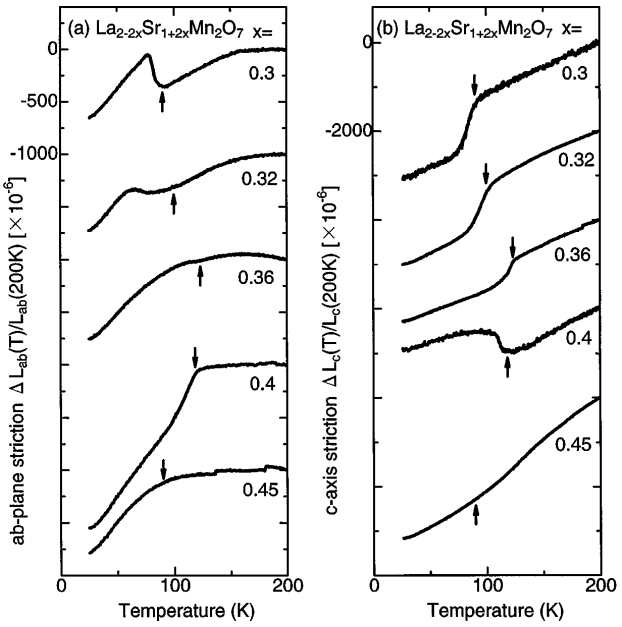

FIG. 2. Temperature dependence of the striction along (a) the ab plane [$\Delta L_{ab}(T)/L_{ab}(200\ \mathrm{K})$] and (b) the c axis [$\Delta L_c(T)/L_c(200\ \mathrm{K})$] in the absence of magnetic fields for $La_{2-2x}Sr_{1+2x}Mn_2O_7$ ($0.3 \leq x \leq 0.45$) crystals. The respective data are vertically offset by every -1000×10^{-6} of $\Delta L_{ab}/L_{ab}$ and -2000×10^{-6} of $\Delta L_c/L_c$ for clear comparison. Arrows indicate the magnetic transition temperature.

lies in the striction at T_c. In the $x = 0.4$ crystal, the striction along the ab plane drops sharply ($\Delta L_{ab}/L_{ab} \sim -0.06\%$) toward lower temperatures at $T_c \approx 120$ K, while the striction along the c axis shows steep increase ($\Delta L_c/L_c \sim 0.05\%$). The results are in good agreement with the abrupt change in the lattice parameters around T_c which was observed by the neutron diffraction measurements ($\Delta a/a \sim -0.08\%$ and $\Delta c/c \sim 0.07\%$) for an $x = 0.4$ sample [11]. The anomaly around T_c is suppressed with increasing x above 0.4. By contrast, in the lower-doped region ($x < 0.36$), we observe a jump of $\Delta L_{ab}/L_{ab}$ and a drop of $\Delta L_c/L_c$ around T_c, i.e., opposite changes to the case of higher doping levels ($x > 0.36$). The change in $\Delta L/L$ is enhanced with decreasing hole concentration. The $x \approx 0.36$ crystal with the highest T_c shows the ferromagnetic (FM) phase but neither expands nor contracts at T_c, apparently positioning at the crossover point between the opposite lattice structural changes. Thus, the spontaneous striction at T_c systematically varies in magnitude, sign, and anisotropy with the doping level. Considering the crystalline data at room temperature [Fig. 1(b)] and the difference in the bandwidth of the respective orbital states [Fig. 1(a)], the orbital-state occupancy of e_g-like electrons is likely relevant to the observed lattice striction.

To verify the above idea, we have investigated the correlation between magnetoelastic phenomena and magnetotransport properties. Figure 3 displays temperature profiles of the resistivity and the striction along the ab plane ($\Delta L_{ab}/L_{ab}$) and the c axis ($\Delta L_c/L_c$) in several

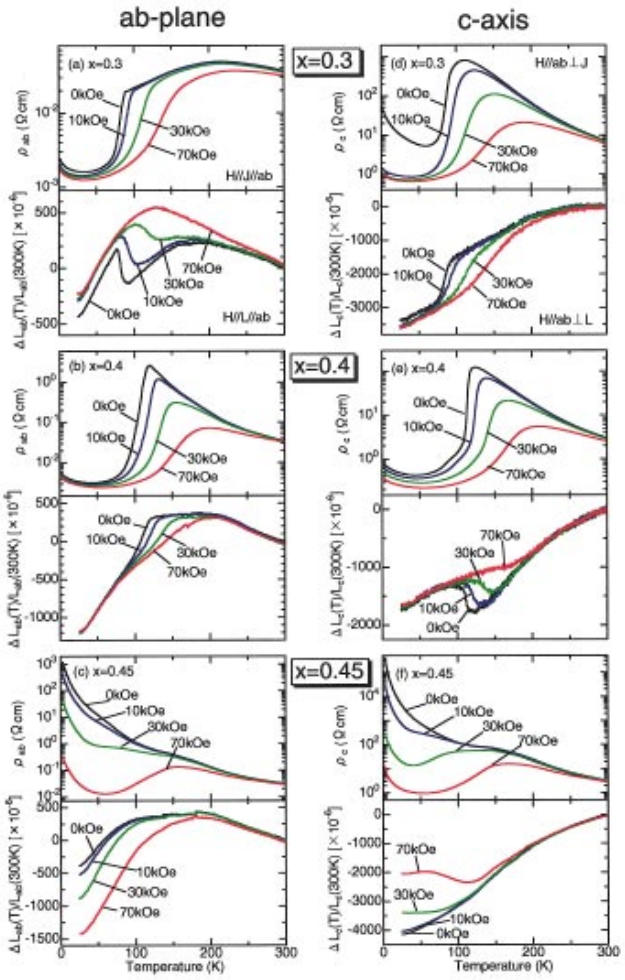

FIG. 3(color). Temperature dependence of [(a)–(c)] in-plane resistivity (ρ_{ab}) and striction $[\Delta L_{ab}(T)/L_{ab}(300\ \mathrm{K})]$ and [(d)–(f)] interplane resistivity (ρ_c) and striction $[\Delta L_c(T)/L_c(300\ \mathrm{K})]$ in several magnetic fields for the $La_{2-2x}Sr_{1+2x}Mn_2O_7$ ($x = 0.3$, 0.4, and 0.45) crystals. The measurements were performed once the magnetic fields are applied at 300 K.

magnetic fields (H) parallel to the ab plane for the crystals with $x = 0.3$, 0.4, and 0.45. All the crystals show gigantic magnetostriction which is closely correlated with the large MR effect, as clearly seen in Fig. 3. A steep drop in resistivity is observed at T_c for $x = 0.3$ and $x = 0.4$ crystals. For the $x = 0.3$ crystal which shows a positive change in spontaneous lattice striction along the ab plane toward the spin-ordered state [Fig. 2(a)], $\Delta L_{ab}/L_{ab}$ considerably increases by applying H above T_c [Fig. 3(a)], whereas $\Delta L_c/L_c$ decreases [Fig. 3(d)]. [The large low-field ($H < 10$ kOe) MR in ρ_c enough below T_c corresponds to the inter-bilayer tunneling MR, as previously argued [3,12].] On the other hand, in the $x = 0.4$ crystal with negative spontaneous lattice striction along the ab plane, $\Delta L_{ab}/L_{ab}$ decreases, yet $\Delta L_c/L_c$ increases by applying H [Figs. 3(b) and 3(e)]. In both the $x = 0.3$ and $x = 0.4$ crystals, the magnetostriction as well as the MR is enhanced around T_c, and becomes small in going away from T_c. However, the sign and magnitude of magnetostriction strongly depend on the doping level. Incidentally, the magnitude of the magnetostriction around T_c is much smaller for an intermediate doped region around $x \approx 0.36$, where a spontaneous striction anomaly at T_c is also small (Fig. 2). Thus, these magnetostriction results are closely related to the spontaneous striction anomaly at T_c.

In the $x = 0.45$ crystal [Figs. 3(c) and 3(f)], both ρ_{ab} and ρ_c show a semiconducting behavior down to the lowest temperature in the absence of H. Two broad anomalies in the resistivity can be observed around 90 and 150 K. The 90 K anomaly is attributed to the onset of the spin-canting. With increasing H, both the ρ_{ab} and ρ_c drastically decrease at low temperatures, and the field-induced insulator-to-metal transition appears to take place. In accordance with the drop of the resistivity by application of H, the lattice striction along the ab plane shrinks and that along the c axis expands, as in the $x = 0.4$ crystal. The temperature dependence of the anisotropic lattice striction as well as that of resistivity shows a similar trace for the $x = 0.4$ and $x = 0.45$ crystals at such a high magnetic field as 70 kOe. The result implies that the field-induced FM spin arrangement is accompanied by a similar lattice striction in such a high-doped region.

We display in Fig. 4 field profiles of $\Delta L_{ab}(H)/L_{ab}(0)$ and $\Delta L_c(H)/L_c(0)$ measured with $H \parallel ab$ at selected temperatures for $x = 0.3$ and 0.4 crystals. For comparison, we show the corresponding MR curves of ρ_{ab} in the lower panels of Fig. 4. As the temperature approaches T_c, the magnitudes of the magnetostriction along the ab plane and the c axis both sharply increase in accordance with

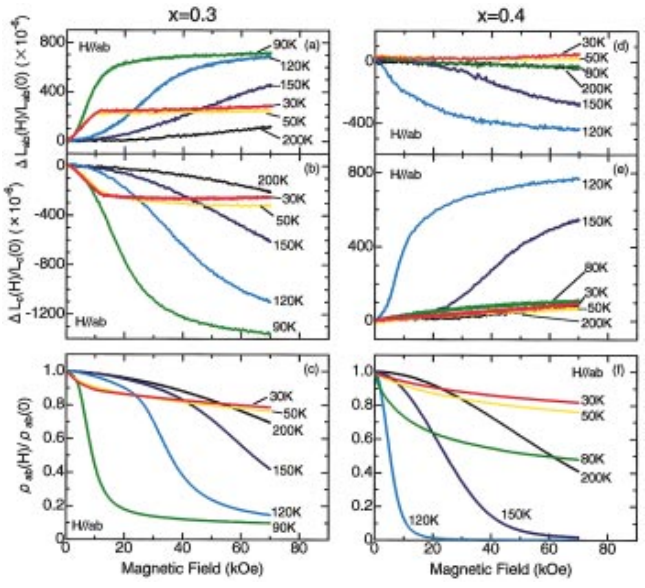

FIG. 4(color). Inplane magnetostriction $[\Delta L_{ab}(H)/L_{ab}(0)]$ (upper), interplane magnetostriction $[\Delta L_c(H)/L_c(0)]$ (middle), and inplane MR $[\rho_{ab}(H)/\rho_{ab}(0)]$ (lower) as a function of H ($H \parallel ab$) at several temperatures for the $La_{2-2x}Sr_{1+2x}Mn_2O_7$ [(a)–(c): $x = 0.3$, and (d)–(f): $x = 0.4$] crystals.

enhancement of MR effect for both crystals. At temperatures near T_c, both $\Delta L_{ab}(H)/L_{ab}(0)$ and $\Delta L_c(H)/L_c(0)$ tend to be saturated at high H. At all temperatures, $\Delta L_{ab}(H)/L_{ab}(0)$ and $\Delta L_c(H)/L_c(0)$ show opposite signs in both crystals. The most striking difference between the $x = 0.3$ and $x = 0.4$ crystals is the sign of the magnetostriction. By applying H, the ab plane expands but the c axis shrinks for $x = 0.3$ crystal, and vice versa for the $x = 0.4$ crystal. Another remarkable difference is that considerable magnetostriction can be observed even enough below T_c only for the $x = 0.3$ crystal. The magnetostriction tends to be saturated at a relatively low field ($\approx$10 kOe) and hence may be related to the rotation of the spin direction from the c axis to the ab plane [14] [see also left panel of Fig. 1(b)]. Comparing the magnetostriction with the MR for the respective cases, one may notice a close interrelation between the magnetotransport and magnetoelastic properties.

To understand the origin of the field-induced striction in the bilayered manganite, we should take account of the orbital degrees of freedom of the e_g-like conduction electrons of Mn^{3+}. Since the orbital character is strongly affected by a lattice form, the observed structural distortion by changing temperature, magnetic field and doping level should reflect sensitively a change in the orbital state. A neutron diffraction study on an $x = 0.4$ sample [11] revealed that the striction effect coupled to the magnetic transition results from changes in individual Mn-O bond lengths of the MnO_6 octahedron. In the case of the heavily doped samples with $x \geq 0.4$, the lattice distortion toward the FM state (or by applying H) has been understood in terms of the stabilization of the $d_{3z^2-r^2}$ orbital state which gives rise to the FM DE interaction along the c axis (z direction). By contrast, the cooling- or field-induced lattice distortion in the lower-doped region of $x \leq 0.36$ appears to stabilize the $d_{x^2-y^2}$ orbital state. Since the MnO_6 octahedron of the bilayered manganite in this compositional region has a collectively JT-distorted structure with elongation along the z direction [Fig. 1(b)], the lattice striction toward the FM state in the lower-doped region tends to suppress such a collective JT distortion. Thus, the FM ordering within a bilayer unit, which is favored by lowering temperature or by applying H, is realized by a *relatively* isotropic mixture of the two orbital states, $d_{x^2-y^2}$ and $d_{3z^2-r^2}$.

The striction behavior in the heavily doped region is rather peculiar. The lattice distortion in the heavily doped region near $x = 1/2$ may be relevant to the charge-orbital ordering as observed in an $x = 0.5$ crystal [9,15]. In the bilayered manganite, the real space ordering of 1:1 Mn^{3+}/Mn^{4+} species accompanies the $d_{3x^2-r^2}/d_{3y^2-r^2}$ orbital ordering of Mn^{3+}, which is frequently observed in manganites with perovskite-related structure. It is possible to speculate that the $d_{3x^2-r^2}/d_{3y^2-r^2}$ orbital ordering is suppressed and altered to a disordered state by applying H. Although there has been no evidence for the static charge-orbital ordering for the incommensurately doped samples with $x = 0.45$ or 0.4, the negative spontaneous lattice striction and magnetostriction along the ab plane are analogous to that for the $n = \infty$ perovskite manganite in the vicinity of the charge ordered state [16,17]. This indicates, at least, the suppression of directional order of e_g orbitals within the ab plane. Thus, the orbital state may crucially vary with magnetic field as well as doping level in the bilayered manganite, which causes the complex doping dependence of magnetostriction as observed.

In summary, we have performed magnetoelastic and magnetotransport measurements to investigate the effect of the spin-charge-orbital coupling in the bilayered manganite crystals, $La_{2-2x}Sr_{1+2x}Mn_2O_7$. We have observed a large spontaneous crystal distortion at T_c as well as a gigantic field-induced striction showing the anisotropy with respect to the crystal axes. The magnetoelastic behaviors are found to systematically vary in sign and magnitude with the doping level, and may be attributed to the field-induced change in the orbital-state occupancy by $d_{x^2-y^2}$, $d_{3z^2-r^2}$, and $d_{3x^2-r^2}/d_{3y^2-r^2}$ states as well as its feedback to the deformation of the MnO_6 octahedron.

We thank Y. Okimoto and R. Kumai for helpful discussions. This work was supported in part by NEDO.

*Present address: Cryogenic Center, University of Tokyo, 2-11-16 Yayoi, Bunkyo-ku, Tokyo 113-0032, Japan.

[1] C. Zener, Phys. Rev. **82**, 403 (1951); P. W. Anderson and H. Hasegawa, *ibid.* **100**, 675 (1955); P.-G. de Gennes, *ibid.* **118**, 141 (1960).
[2] Y. Moritomo *et al.*, Nature (London) **380**, 141 (1996).
[3] T. Kimura *et al.*, Science **274**, 1698 (1996).
[4] J. F. Mitchell *et al.*, Phys. Rev. B **55**, 63 (1997).
[5] P. D. Battle *et al.*, Chem. Mater. **9**, 1042 (1997).
[6] T. Kimura *et al.*, Phys. Rev. Lett. **79**, 3720 (1997).
[7] D. S. Dessau *et al.*, Phys. Rev. Lett. **81**, 192 (1998).
[8] N. Hamada *et al.* (unpublished). To be accurate, the two orbital components, $d_{x^2-y^2}$ and $d_{3z^2-r^2}$ are mixed at general k points apart from the high-symmetry points, (0,0) and (π,π).
[9] T. Kimura *et al.*, Phys. Rev. B **58**, 11 081 (1998).
[10] J. F. Mitchell *et al.*, Mater. Res. Soc. Symp. Proc. **453**, 343 (1997).
[11] D. N. Argyriou *et al.*, Phys. Rev. B **55**, R11 965 (1997).
[12] T. G. Perring *et al.*, Phys. Rev. B **58**, R14 693 (1998).
[13] K. Hirota *et al.*, J. Phys. Soc. Jpn. **67**, 3380 (1998).
[14] We have measured the field-direction dependence of the magnetostriction. The application of H along the c axis gave rise to smaller magnitude of the saturation magnetostriction below T_c for $x = 0.3$ crystal but larger one for $x = 0.4$ crystal than that along the ab plane.
[15] J. Q. Li *et al.*, Phys. Rev. B **57**, R3205 (1998).
[16] M. R. Ibarra *et al.*, Phys. Rev. Lett. **75**, 3541 (1995); M. R. Ibarra *et al.*, Phys. Rev. B **57**, 7446 (1998).
[17] H. Kuwahara *et al.*, Phys. Rev. B **56**, 9386 (1997).